1 BI layer upgrade

1.1 sMDT chambers

The ATLAS Monitored drift tube (MDT) chambers provide reliable muon tracking with excellent spatial resolution and high tracking efficiency independent of the track incident angle. Small-diameter muon drift tube (sMDT) chambers [1] with a tube diameter of 15 mm, i.e. half of the tube diameter of the MDT chambers, have been developed since 2008 to cope with the higher background irradiation rates at HL-LHC and to allow for more tube layers or additional trigger chambers under the tight space constraints in the muon spectrometer. Standard aluminium tubes with 0.4 mm wall thickness like for the MDT chambers are used. Figure 1 shows a comparison of the MDT and the sMDT drift tubes. The sMDT chambers are operated in ATLAS with the same gas, gas pressure and gas gain as the MDT chambers. Table 1 shows a comparison of the MDT and sMDT operating paremters. The drift time spectra are shown in the left-hand part of Figure 2. The maximum drift time of the sMDT tubes is only 175 ns compared to about 720 ns of the MDT chambers leading, together with the twice smaller cross section exposed to the radiation, to about 8 times lower occupancy and a linear space-to-drift time relationship with the standard MDT drift gas Ar:CO_2 (93:7) at 3 bar pressure.

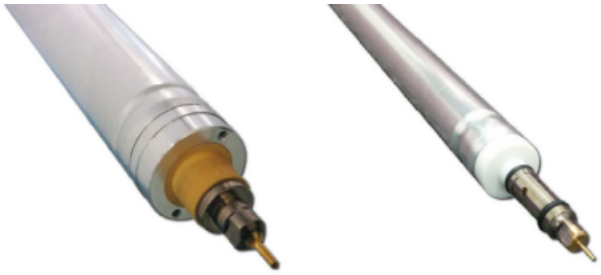

Figure 1: Picture of MDT (left) and sMDT (right) tubes.

A full-scale sMDT prototype chamber of trapezoidal shape has been constructed and tested in the H8 muon beam and in the Gamma Irradiation Facility (GIF) at CERN in 2010 [2]. The chamber has been operated in the ATLAS cavern in 2012. In 2014, two BME sMDT chambers [3] have been installed in the elevator regions of the barrel muon spectrometer, each with two new RPC chambers, and are in operation since the start of LHC Run 2 [4]. In January 2017, 12 BMG sMDT chambers [5], have been installed in the detector feet in sectors 12 and 14 of the barrel muon spectrometer [4, 6].

The construction of 16 BIS 7/8 sMDT chambers with integrated triple thin-gap RPC chambers has started. They will be installed at the ends of the BIS layers in the barrel inner layer in LS2 2019-20 in order to improve the trigger efficiency and the rate capability of the chambers in the transition regions between barrel and endcaps [7]. This phase 1 upgrade serves as pilot project for the complete replacement of the BIS 1-6 MDT chambers by sMDT-RPC chamber modules of very similar design as the BIS7/8 chambers in LS3. Together with the installation of additional thin-gap RPCs on the BIL MDT chambers, the robustness of the barrel muon trigger system will be greatly enhanced over the full lifetime of the experiment at the high irradiation rates at HL-LHC. The installation of new BIS triple thin-gap RPCs of only 5 cm thickness becomes possible only by replacing the BIS MDT chmabers by sMDT chambers which have about half the height. In addition, the sMDT chambers provide about an order of magnitude higher rate capability than the MDTs.

1.2 Performance of the sMDT chambers

The performance of MDT and sMDT chambers has been extensively studied at the Gamma Irradiation Facility at CERN using the existing ATLAS MDT readout electronics with bipolar

Table 1: Material and operating parameters of ATLAS sMDT chambers compared to the MDT chambers. 500 Hz/cm^2 and 200 kHz/tube are the maximum background rates expected in the barrel inner layer of the ATLAS muon spectrometer at HL-LHC.

Type	MDT	sMDT
Tube material	Aluminium Aluman100	Aluminium AW 6060-T6/ AlMgSi
Tube inner&outer surface		Surtec 650 chromatisation
Tube outer diameter	29.970 mm	15.000 mm
Tube wall thickness	0.4 mm	0.4 mm
Wire material	W-Re (97:3)	W-Re (97:3)
Wire diameter	50 μm	50 μm
with gold plating thickness	3%	3%
Wire pitch	30.035 mm	15.099 mm
Wire tension	350 ± 15 g	350 ± 15 g
Gas mixture	Ar:CO_2 (93:7)	Ar:CO_2 (93:7)
Gas pressure	3 bar (abs.)	3 bar (abs.)
Gas gain	$2 \cdot 10^4$	$2 \cdot 10^4$
Wire potential	3080 V	2730 V
Maximum drift time	720 ns	175 ns
Average tube spatial resolution without backgr. irradiation	83 μm	106 μm
Average tube spatial resolution at 500 Hz/cm^2 backgr. rate	160 μm	110 μm
Drift tube muon efficiency without backgr. irradiation	95%	94%
Drift tube muon efficiency at 200 kHZ/tube backgr. rate	80%	90%
Wire positioning accuracy	20 μm rms	20 μm rms

shaping [8, 1, 9]. For the (s)MDT amplifier-shaper-discriminator (ASD) chips at HL-LHC the same specifications will be used as for the present system. The MDT chambers can be operated up to background rates of 500 Hz/cm^2 and 300 kHz per tube. At background rates above 500 Hz/cm^2, the gas gain drops by more than 20% (see Figure 2, right) leading, together with the effect of space charge fluctuations, to rapid deterioration of the spatial resolution with increasing background flux. The limitations of the MDT chambers are overcome by using drift tubes with half the diameter of the ATLAS MDT tubes while leaving the operating parameters, Ar:CO_2 (93:7) gas mixture at 3 bar pressure and nominal gas gain of 20000 (for a wire potential with respect to the tube wall of 2730 V in sMDT tubes), unchanged [1].

As the space charge density inside the drift tubes is proportional to the third power of the tube radius, 15 mm diameter drift tubes show a significant gain drop only at 8 times higher background rates compared to 30 mm diameter drift tubes (see Figure 2, right). At the same time, the deteriorating effect of space charge fluctuations on the spatial resolution is eliminated because the drift gas is linear to good approximation for drift radii below 7.5 mm (see Figure 3, left). The radial dependence of the spatial resolution of 15 and 30 mm diameter drift tubes from measurements in the H8 muon beam at CERN without radiation background is shown in the right-hand part of Figure 3 [10]. Standard MDT time-slewing corrections are applied in both cases. Without irradiation and associated space charge effects and with time-slewing corrections, the average sMDT drift tube resolution is 106 ± 2 μm compared to 83 ± 2 μm for the MDTs [10]. The dependence of the average spatial resolution of MDT and sMDT drift tubes

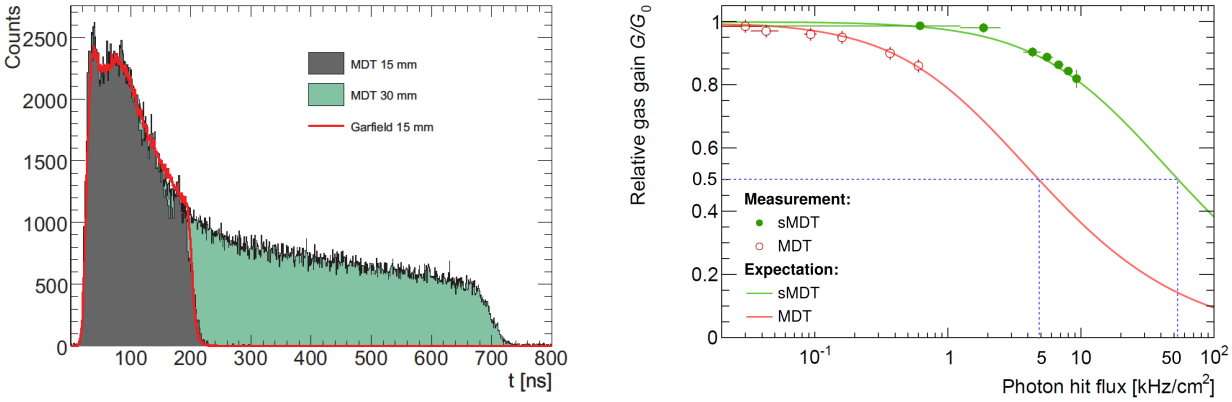

Figure 2: Left: Drift time spectra of MDT (green) and sMDT tubes (grey) together with the prediction of a GARFIELD simulation for sMDT tubes (red line) [1]. Right: Measurements of the gas gain of MDT and sMDT tubes relative to the nominal gas gain $G_0 = 20000$ as a function of the γ background rate at the Gamma Irradiation Facility at CERN compared to predictions based on the Diethorn formula [10].

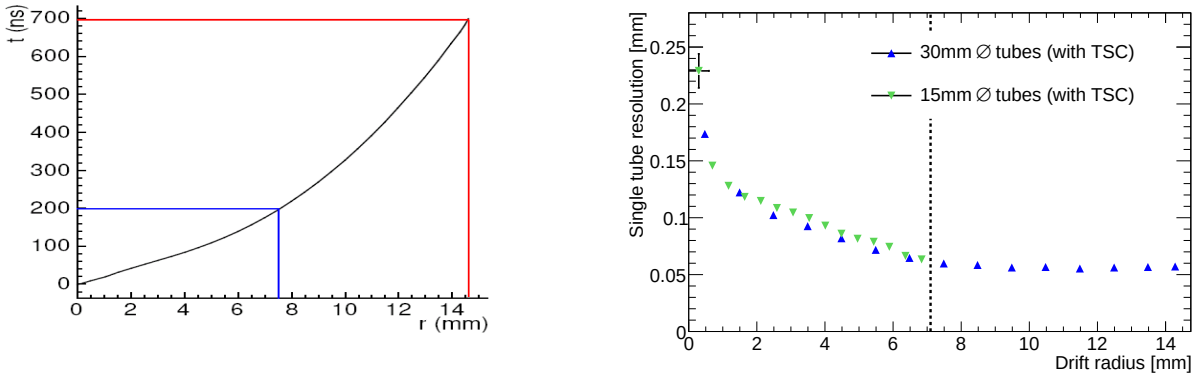

Figure 3: Left: Track radius-to-drift time relationship of MDT drift tubes. The part with drift radii r below 7.5 mm, relevant for the sMDT tubes, is linear to good approximation. Right: Spatial resolution after time slewing corrections (TSC) as a function of the drift radius for MDT and sMDT drift tubes measured under the same operating conditions in the H8 muon beam at CERN without background irradiation [9, 10]. As expected, the results for 15 and 30 mm diameter tubes are in good agreement for drift radii below 7.5 mm.

on the γ background rate is shown in Figure 4. The spatial resolution deteriorates quickly with increasing background flux for the MDTs while it is affected only little by space charge effects up to very high irradiation rates for the sMDTs.

At the same background rate, the small-diameter drift tubes experience 8 times lower occupancy than the 30 mm diameter MDT tubes because of the 4 times shorter maximum drift time (see Figure 2) and the twice smaller tube cross section exposed to the radiation. Because of the much shorter maximum drift time, the dead time of the MDT readout electronics (which for the MDTs is set to a nominal value of 820 ns, slightly above the maximum drift time, to prevent the detection of secondary ionization clusters) can be reduced to the minimum adjustable value of 220 ns, just above the maximum drift time of the sMDT tubes. In this way, the masking of muon hits by preceding background pulses is strongly reduced increasing the muon detection efficiency defined as the probability to find a hit on the extrapolated muon track within 3 times

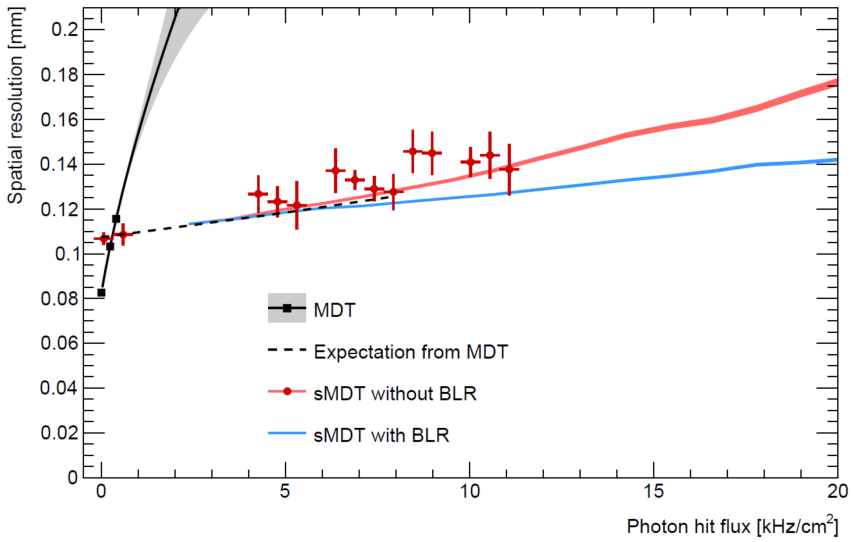

Figure 4: Average spatial resolution of MDT and sMDT drift tubes as a function of the γ background fluence rate measured at the Gamma Irradiation Facility at CERN.

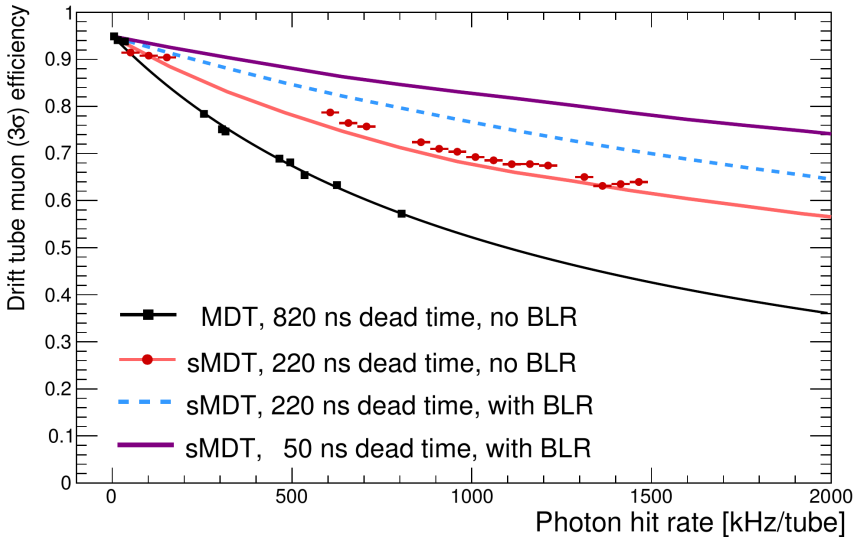

Figure 5: Muon detection efficiencies of MDT and sMDT drift tubes with corresponding electronics deadtime settings (see text) as a function of the γ background counting rate per tube. The efficiency is defined as the probablity to find a hit on the extrapolated track within 3σ of the drift tube spatial resolution (3σ efficiency). The measurement results agree well with the expectations from detailed simulations of detector and electronics response.

the drift tube resolution (3σ efficiency). Figure 5 shows the improvement of the 3σ efficiency of sMDT tubes at high background counting rates compared to the MDT tubes. Muon track segment reconstruction efficiencies of almost 100% and a spatial resolution of better than 30 μm are achieved with 8-layer sMDT chambers at the maximum background rates expected at HL-LHC.

1.3 Drift tube design and fabrication

The sMDT chamber design and construction procedures have been optimized for mass production while they provide highest mechanical accuracy in the sense wire positioning. Standard industrial aluminium tubes with 15 mm outer diameter and a wall thickness of 0.4 mm are used. The tubes are chromatised on the in- and outside for the cleaning purposes and reliable electrical ground contact. The ground pins are screwed into the holes between adjacent tube

Figure 6: Semi-automated drift-tube assembly station in a climatised clean room.

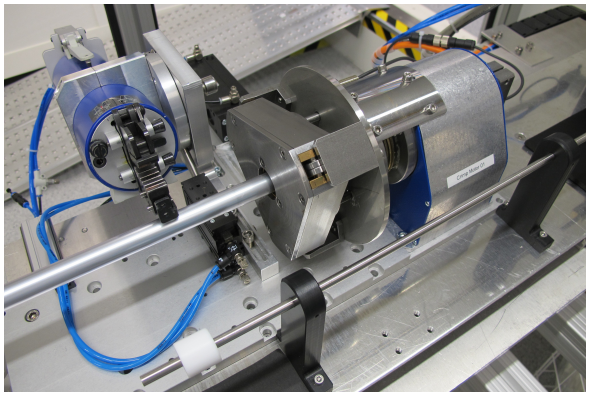

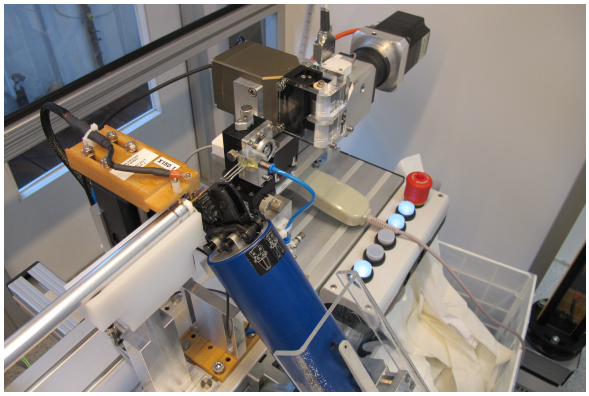

Figure 7: Automated tools for the mechanical swaging of the aluminium tubes onto the O-rings on the endplugs (see Figure 8) for fixation and gas sealing (left) and for crimping of the sense wire in heat-treated copper crimp tubelets inserted into the central brass pins of the endplugs (right). This operation takes place after the feeding of the wire through the tube by air flow, without manual interference, and after automated tensioning of the wire using a stepping motor controlled by a strain gauge (right).

triplets during the glueing of the tube layers (see Figure 8). The drift tube design and fabrication procedures are the same as used for the construction of the BMG sMDT chambers in 2016 [5, 11].

The drift tubes are assembled using a semi-automated wiring station in a temperature-controlled clean room (see Figure 6). The endplugs are inserted into the tubes and the sense wires fed through the tubes and the endplugs (see Figs. 8 and 9) by means of air flow without manual contact. Afterwards the endplugs are fixed and and the tubes gas sealed by swaging (see Fig. 7). Finally, the wires are fixed in copper crimp tubelets inserted in the endplug central

pins after tensioning them to 350 ± 15 g (see Fig. 7, right) corresponding to a gravitational sag of only 17 ± 1 μm (absolute tolerances) including overtensioning to 430 g for 10 s. The wires are positioned at each tube end with a few micron precision with respect to a cylindrical external reference surface on the central brass insert of the endplug which also holds the spiral shaped wire locator on the inside of the tube. The drift tubes are sealed with the endplugs using two O-rings per endplug and mechanical swaging of the tube walls. For the injection molded endplug insulators and gas connectors for the individual tubes, plastic materials with minimum outgassing have been selected which are also immune against cracking.

A full-scale sMDT prototype chamber of trapezoidal shape has been constructed and tested in the H8 muon beam and in the Gamma Irradiation Facility (GIF) at CERN in 2010 [2]. The chamber has been operated in the ATLAS cavern in 2012. In 2014, two BME sMDT chambers [3] have been installed in the elevator regions of the barrel muon spectrometer, each with two new RPC chambers, and are in operation since the start of LHC Run 2 [4]. In January 2017, 12 BMG sMDT chambers [5], have been installed in the detector feet in sectors 12 and 14 of the barrel muon spectrometer [4, 6].

The construction of 16 BIS 7/8 sMDT chambers with integrated triple thin-gap RPC chambers has started. They will be installed at the ends of the BIS layers in the barrel inner layer in LS2 2019-20 in order to improve the trigger efficiency and the rate capability of the chambers in the transition regions between barrel and endcaps [7]. This phase 1 upgrade serves as pilot project for the complete replacement of the BIS 1-6 MDT chambers by sMDT-RPC chamber modules of very similar design as the BIS7/8 chambers in LS3. Together with the installation of additional thin-gap RPCs on the BIL MDT chambers, the robustness of the barrel muon trigger system will be greatly enhanced over the full lifetime of the experiment at the high irradiation rates at HL-LHC. The installation of new BIS triple thin-gap RPCs of only 5 cm thickness becomes possible only by replacing the BIS MDT chmabers by sMDT chambers which have about half the height. In addition, the sMDT chambers provide about an order of magnitude higher rate capability than the MDTs.

Only materials already certified for the ATLAS MDT chambers are used for sMDT drift tubes and their gas connections in order to prevent ageing. No outgassing of the plastic materials of endplugs (PBTP Crastin LW9330, reinforced with 30% glass fiber) and gas connectors (PBTP Crastin S600F20, unreinforced) has been observed. The sMDT tubes, including the plastic material of the endplugs, have been irradiated with a 200 MBq ^{90}Sr source over a period of 4 months with a total charge accumulation on the sense wire of 9 C/ cm without any sign of ageing [10, 12].

Typical production rates of 100 tubes per day have been achieved with one assembly station operated by two technicians at an average failure rate of about 4%, which is mostly due to occasional failures of the assembly devices [13]. During the production of the 4300 BMG drift tubes, the failure rate of the standard drift tube quality tests of wire tension (350 ± 15 g), gas leak rate ($< 10^{-8}$ bar l/s) and leakage current (< 2 nA/m) at the nominal operating voltage of 2730 V was only 2% [13], mostly due to too high dark currents under high voltage.

1.4 sMDT chamber construction and test

After passing the quality assurance tests, the drift tubes are assembled to chambers in a climatised clean room by inserting the endplug reference surfaces into a grid of fitting bores in the assembly jigs at each chamber end which define the wire positions with an accuracy of better than 5 micron (see Figure 10) and glueing them together and to the spacer and support frame using an automated glue dispenser (see Figure 11). A complete chamber can be assembled within two working days, including the precise mounting of the global alignment sensor platforms. The precisely machined assembly jig used for the BIS 7/8 chambers, which will also be used for the BIS 1-6 chambers, is shown in Figures 12, 13 and 14. The same two-component expoxy glues as for the MDT chamber construction are used, Araldite 2014 between the tube layers

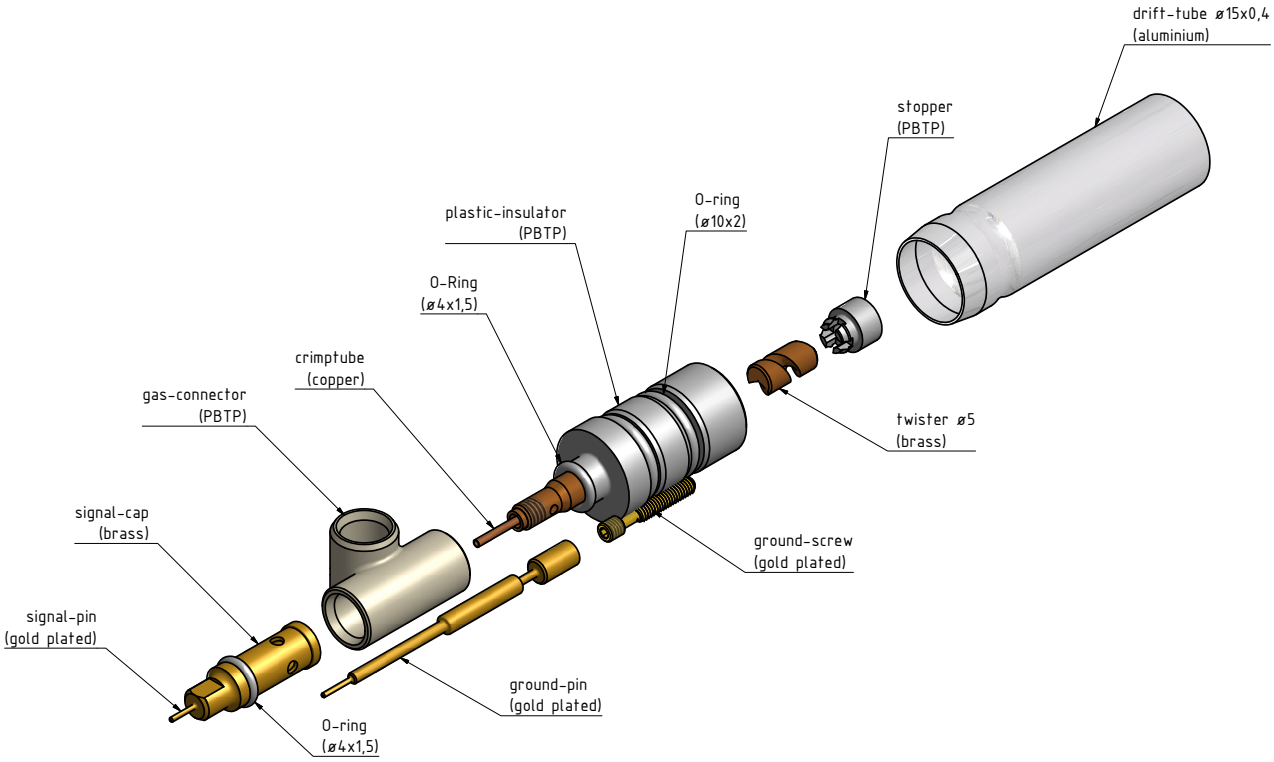

Figure 8: Exploded view of an sMDT endplug with interfaces for precise wire positioning and measurement, for gas and high-voltage supplies and for readout electronics [2].

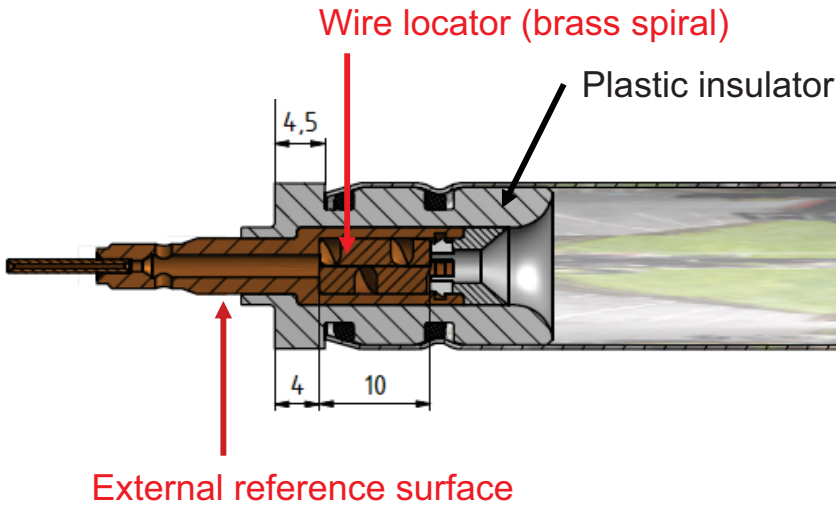

Figure 9: Cross section of an sMDT endplug with internal wire locator and external reference surface for tube and wire positioning during construction and for wire position measurement [5].

and DP 490 between multilayers and spacer and support structures. After the glueing of each new tube layer, ground connection screws are inserted into the triangular gaps between adjacent tube layers through holes in the jig, scratching the chromatised tube walls. The gaps are filled with glue during the assembly of the next layer, fixing and encapsulating the ground screws.

Conducting glue may be added in order to improve the conductivity of the ground connection if necessary. After mounting of the gas connections, ground pins connecting to the readout and high-voltage distribution boards are screwed onto the ground screws (see Figure 15).

Like the BME sMDT chambers, but in contrast to the BMG chambers, the BIS7/8 and BIS 1-6 sMDT chambers will have in-plane alignment monitoring systems. The longitudinal sag monitors of the in-plane alignment system of the BIS 7/8 chambers is rotated by 180° with respect to the standard orientation parallel to the tube direction in the MDT and also the BME and BIS 1-6 chambers in order to properly monitor potential deformations of the complex shaped chambers transverse to the tubes. Two diagonal straightness monitors measure torsions between the readout and high-voltage ends in all types of chambers. In addition to the axial, praxial and CCC alignment sensors which are mounted on the outer multilayer of all new BIS sMDT chambers in the same positions as on the present BIS MDT chambers, the BIS 7/8 chambers carry barrel-endcap alignment sensors on the inner multilayer connecting to the NSWs (see Figure 16). The global alignment sensors are mounted with 20 μm positioning accuracy with respect to the sense wires on the outer tube layers using the precision assembly jigging (see Figure 12).

After the glueing of the tube layers, the positions of the individual endplug reference surfaces and, thus, of the sense wires are measured at the two chamber ends with an automated coordinate measuring machine with a precision of about 2 μm (see Figure 17). The measurement was performed within 1-2 hours for every BME and BMG chamber and is planned as regular spot check during the BIS chamber serial production. In particular, the positions of the alignment sensor platforms with respect to the wire grid can be measured with a few micron accurracy. Sense wire positioning accuracies of better than 10 μm (rms) have been routinely achieved during BME and BMG chamber construction [4, 5]. An ultimate wire positioning accuracy of 5 µm (rms) has been achieved in BMG chamber construction which reaches the precision of the assembly jigs (see Figure 18). After the measurement, the individual wire positions are known with 2 μm accuracy.

After the wire position measurement, the parallel gas distribution system is mounted, consisting of modular injection molded plastic gas connectors connecting tubes in columns perpendicular to the chamber plane to the chromatised aluminium gas distribution bars (see Figures 8 and 19). Gas leak rates at 3 bar pressure below the limit of $2n \cdot 10^{-8}$ bar l/s required for a chamber with n tubes have been achieved for all BMG chambers [5]. Minor modifications of the gas connectores and gas bars had to be implemented due to the small available space in the BIS layer. The new injection molded connectors have been produced and sucessfully tested (see Figure 20).

1.5 sMDT chamber electronics

After the installation of the gas distribution system and ground pins, the Faraday cages and the high-voltage distribution boards and the signal distribution boards (see Figure 21) as well as the active readout electronics boards (mezzanine cards) with 6 x 4 readout channels matching the transverse cross section of the quadruple-multilayers are mounted on the HV and the RO side, respectively (see Figures 22 and 23). The decoupling capacitors on the RO side and the terminating resistors on the HV side are enclosed in plastic containers in order to guarantee HV stability. The mezzanine cards stacked on top of the signal distribution boards contain three 8-channel ASD chips and a TDC chip which digitises the threshold crossing times of the signal pulses, multiplexes the data and transmits them to the CSM (chamber service module) via flat twisted-pair signal cables (blue cables in Figure 24) which fulfill the same specifications as the MDT signal cables. as well as a CERN HPTDC chip [14] and a FPGA for the JTAG programming, respectively. They provide the same functionality as the standard MDT readout electronics. The stacked sMDT readout boards used for the BMG and, until the end of LHC phase 1, for the BIS 7/8 chambers are shown in Figure 15). They contain three of the current

MDT ASD chips together with a CERN HPTDC chip [14] as well as an FPGA for JTAG programming and provide the same functionality as the MDT mezzanine cards. The same board layout with the new versions of the ASD and TDC chips in 130 nm CMOS technology will be used for the sMDT chambers in LHC phase 2.

1.6 BIS sMDT chamber design

Table 2: Geometrical parameters of the BIS 1-6 sMDT chambers

Type	BIS 1	BIS 2-6
Number of chambers	16	80
Radial distance from beam axis (mm)	4550 (4635)*	4550 (4635)*
Chamber width in z (mm)	1113	933
Tubes width in z (mm)	1081	901
Chamber length in x (mm)	1839	1839
Aluminium tube length (mm)	1660	1660
Assembled tube length (mm)	1669	1669
Active tube length (mm)	1640	1640
Active area/chamber (m^2)	1.77	1.48
Tube layers	2 x 4	2 x 4
Tubes/layer	71	59
Tubes/chamber	568	472
Spacer height (mm)	45.6	45.6
Tubes height (mm)	139	139
Chamber height (mm)	249	249
Gas volume/chamber (l)	151	126
Chamber weight (kg)	100	86
Mezz. cards (24 ch.)/chamber	24	20
Mezz. cards/CSM 1 (inner ML1)	12	10
Mezz. cards/CSM 2 (outer ML2)	12	10
CSMs/chamber	2	2
T-sensors/chamber	10	10
B-field sensors/chamber	2	2
In-plane alignment systems/chamber	4	4
Axial alignment sensors/chamber	2	4
Praxial alignment sensors/chamber	4	8
CCC alignment sensors/chamber	0	2
Survey targets/chamber	4	4

* Numbers in brackets refer to sectors 2 and 16.

The design and construction of new BIS78 sMDT chambers with 2 x 4 tube layers and integrated thin-gap RPCs with three gas gaps for the replacement of the current BIS 7 and BIS 8 MDT chambers in the 2019-20 LHC shutdown is a pilot project for the complete replacement of the BIS MDT chambers by integrated sMDT and RPC chambers for HL-LHC. There are 12 different types of BIS 78 sMDT chambers with complex shapes maximising the coverage in the overlap region with the New Small Wheels [15]. The drawings of a BIS 7/8 sMDT chamber are shown in Figure 16. The design of the remaining new BIS 1-6 sMDT and RPC chambers will be very similar to the BIS 7/8 design, with the simplifications of rectangular shape and only two chamber types differing in their width in z direction. The parameters of the BIS 1-6 sMDT chambers are summarised in Tables 2 and 3. The same assembly procedure and precision tooling will be used both for the BIS 7/8 and for the BIS 1-6 sMDT chambers.

Table 3: BIS 1-6 sMDT chambers in numbers

Parameter	Value
Number of chambers	96
Number of tubes	37248
Total tube and wire length	63.1 km
Chamber active area	145 m^2
Gas volume	12.3 m^3
Chamber weight	8.5 t
Number of mezzanine cards	1984
Number of hedgehog boards	3968
Number of CSMs	192

The common challenge for the mechanical design is the small available space to be shared with the new RPC chambers and the control of gravitational deformations of the thin chambers with minimal space for support structure. The RPC chambers are mounted on their own support frame and will be installed on the existing rails in the BIS layer independently from the sMDTs to prevent distortion of the BIS sMDT chambers. The BIS 1-6 sMDT chambers are each reduced in width by one drift tube per layer compared to the maximum possible to provide a gap of 20 mm between adjacent chambers which allows for the passage of the RPC rail supports. The chamber readout service modules (CSMs) will be mounted on the toroid coils as close as possible to each chamber such that the signal cable length between mezzanine cards and CSMs will not be longer than 4 m which is still acceptable for realiable signal transmission.

References

[1] B. Bittner et al., *Development of Muon Drift-Tube Detectors for High-Luminosity Upgrades of the Large Hadron Collider*, arXiv:1603.09504, June 2009, Nucl. Instrum. and Meth. **A617** (2010) 169;

[2] H. Kroha et al., *Construction and test of a full-scale prototype drift-tube chamber for the upgrade of the ATLAS muon spectrometer at high LHC luminosities*, Nucl. Instrum. and Meth. A718 (2013) 427.

[3] G. Aielli et al., *Proposal for the Upgrade of the Elevator Regions in the ATLAS Barrel Muon Spectrometer*, ATL-MUON-INT-2014-001, November 2013.

[4] C. Ferretti, H. Kroha (on behalf of the ATLAS muon collaboration), *Upgrades of the ATLAS Muon Spectrometer With sMDT Chambers*, proceedings of the 13^{th} Pisa Meeting on Advanced Detectors, La Biodola, Isola d'Elba, Italy, 24–30 May 2015, arXiv:1603.09544, June 2015, Nucl. Instrum. and Meth. **A 824** (2016) 538.

[5] H. Kroha et al., *Construction and Test of New Precision Drift Tube Chambers for the ATLAS Muon Spectrometer*, arXiv:1603.08760, March 2016, Nucl. Instrum. and Meth. A, doi:10.1016/j.nima.2016.05.091.

[6] H. Kroha, *Proposal for the Improvement of the ATLAS Muon Spectrometer Momentum Resolution in Barrel Sectors 12 and 14*, ATL-MUON-INT-2015-001, February 2015.

[7] G. Aielli et al., *The BIS78 Project*, ATLAS Internal Note, ATL-MUON-INT-2015-xxx, February 2015.

[8] M. Deile et al., *Resolution and Efficiency of the ATLAS Muon Drift-Tube Chambers at High Background Rates*, Nucl. Instrum. and Meth. **A535** (2004) 212; S. Horvat et al., *Operation of the ATLAS Muon Drift-Tube Chambers at High Background Rates and in Magnetic Fields*, IEEE Trans. Nucl. Sci., Vol. 53, No. 2 (2006) 562.

[9] B. Bittner, *Development and Characterisation of New High-Rate Muon Drift Tube Detectors*, PhD thesis, Technical University Munich, MPI Report, MPP-2012-130, CERN-THESIS-2012-122, Juli 2012; P. Schwegler, *High-Rate Performance of Muon Drift Tube Detectors*, CERN-THESIS-2014-091. PhD thesis, Technical University Munich, MPI Report, MPP-2014-302, CERN-THESIS-2014-091, Juli 2014.

[10] B. Bittner et al., *Performance of drift-tube detectors at high counting rates for high-luminosity LHC upgrades*, Nucl. Instrum. Meth. **A732** (2013) 250.

[11] H. Kroha et al., *Performance of New High-Precision Muon Tracking Detectors for the ATLAS Experiment*, Conference Record 2016 IEEE Nuclear Science Symposium, Strasbourg, France, 29 October–6 November 2016, NSS-2016-N22-3, arXiv:1701.08971, November 2016; H. Kroha, A. Kozhin, R. Fakhroutdinov, *New High-Precision Drift-Tube Detectors for the ATLAS Muon Spectrometer*, proceedings of the Instrumentation for Colliding Beam Physics INSTR17 conference, 27 February-3 March 2017, Novosibirsk, Russia, arXiv:xxxx.xxxxx, May 2017.

[12] O. Kortner et al., *Precision Muon Tracking Detectors and Read-Out Electronics for Operation at Very High Background Rates at Future Colliders*, Nucl. Instr. and Meth. **A824** (2016) 556.

[13] H. Kroha et al., *Design and Construction of the BMG sMDT Chambers for the ATLAS Muon Spectrometer*, ATL-COM-MUON-2017-xxx, May 2017.

[14] J. Christiansen et al., *HPTDC–High Performance Time to Digital Converter, Version 1.3*, CERN/EP-MIC, March 2004, https://cds.cern.ch/record/1067476/files/cer-002723234.pdf.

[15] H. Kroha, *sMDT Chamber Parameter Book*, ATL-COM-MUON-2017-xxx, May 2017.

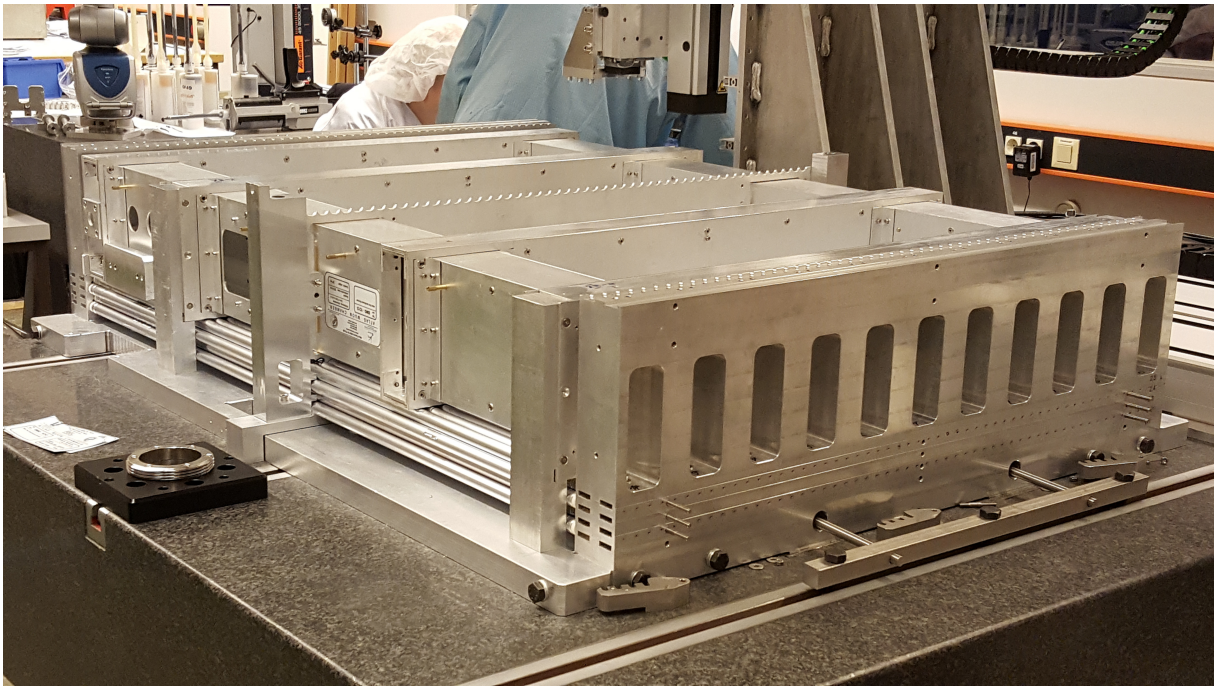

Figure 10: Assembly of a BMG sMDT chamber. The first multilayer has been assembled, the alignment sensor platforms have been mounted on the inside of the multilayer and the spacer frame is positioned on top, waiting for the assembly of the second multilayer on top. The wire grids at each chamber end are defined by the precisely machined grids of holes into which the cylindrical endplug reference surfaces are inserted. The tube and corresponding jig layers are stacked, including the spacing between the two multilayers.

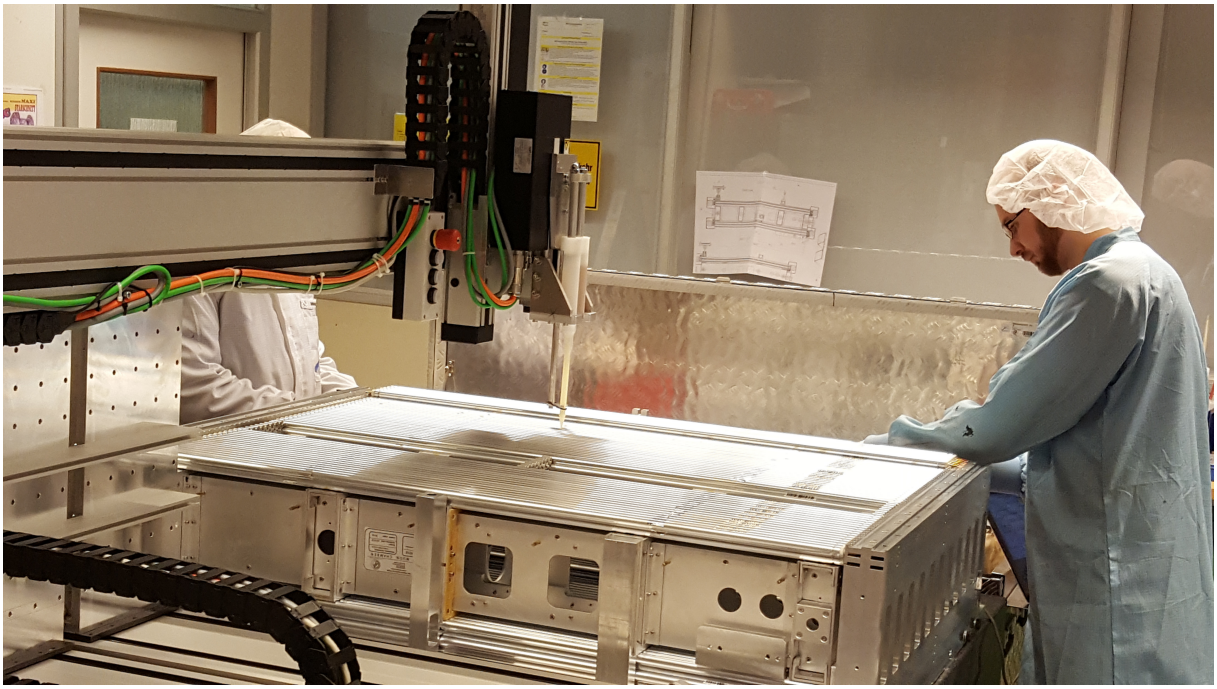

Figure 11: Glue distribution between adjacent tubes of a tube layer during BMG chamber assembly (second multilayer) using an automated glue dispenser.

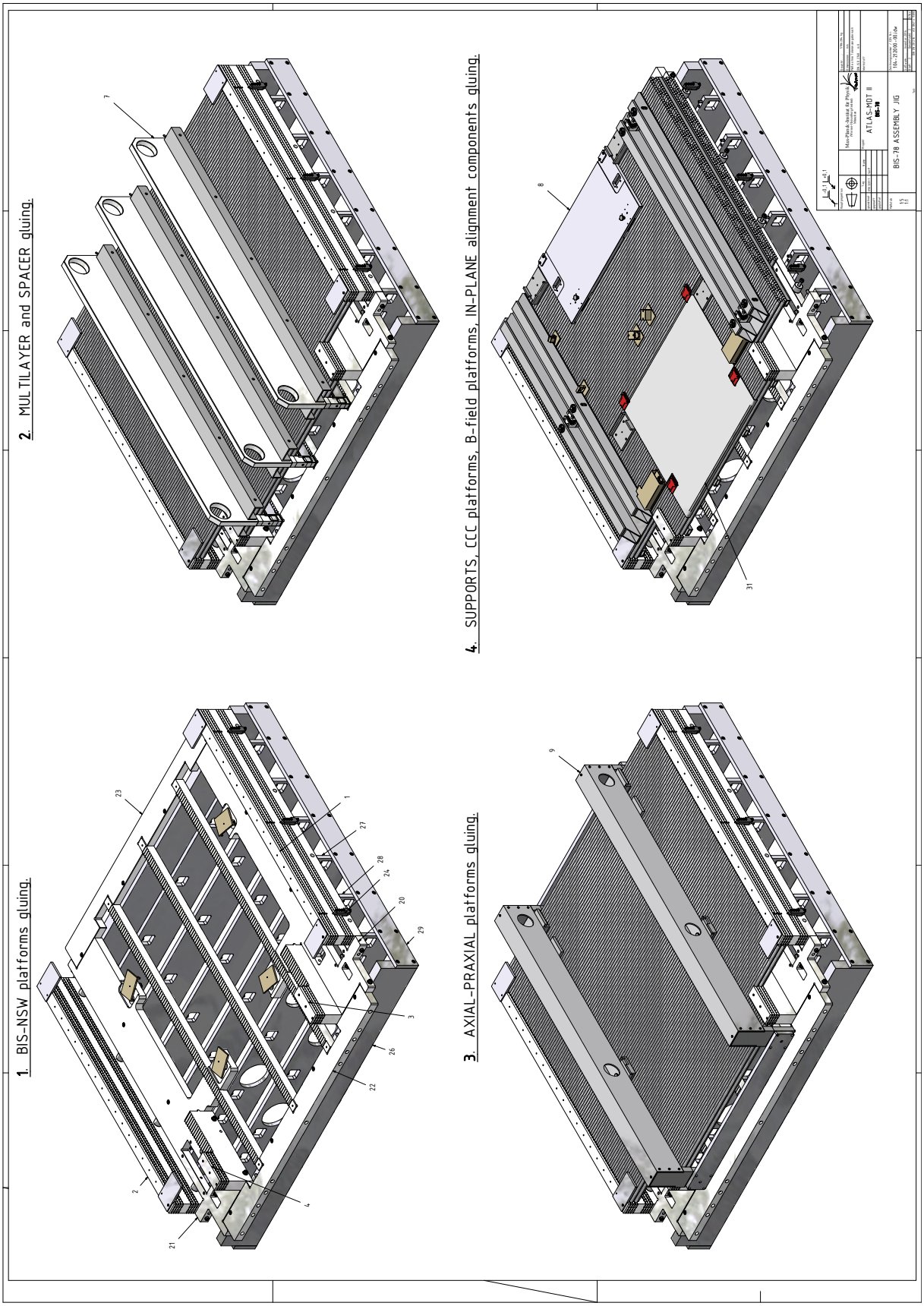

Figure 12: Sketch of the precision jigging and illustration of the steps of the BIS 7/8 and BIS 1-6 chamber assembly procedure. The brackets for the precise mounting of the global alignment sensor platforms are an integral part of the jigging design. The sensors for alignment with respect to the NSWs are mounted to the bottom of the first multilayer in the first step and are only present for BIS 7/8. The axial, praxial and CCC alignment sensors are mounted, together with the in-plane alignment system on the outside of the top multilayer during chamber assembly.

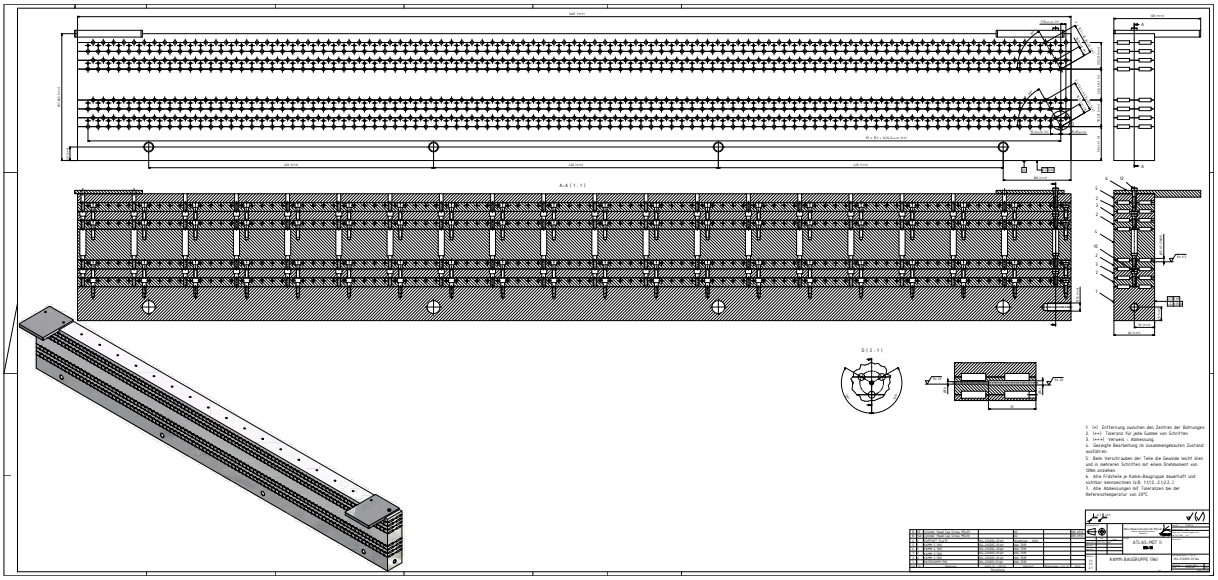

Figure 13: Drawing of the assembly jig for the BIS 1-8 chambers with the precision machined hole grids for the insertion of the endplugs of the drift tubes.

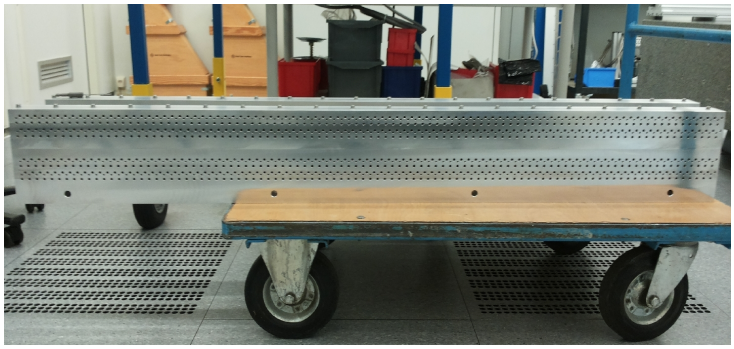

Figure 14: Photograph of the assembly jig for the BIS 1-8 chambers with the precision machined hole grids for the insertion of the endplugs of the drift tubes.

Figure 15: Left: sMDT signal distribution board with stacked mezzanine card carrying three ASD chips (middle layer) and the HPTDC with programming FPGA (top layer). The coupling capacitors to the signal pins of the drift tubes are encapsulated in injection molded white plastic containers to ensure high-voltage stability. The gold-plated signal pins and ground pins are inserted into receptacles on the signal distribution boards which also contain the protection network for the ASD chips. The passive signal distribution (hedgehog) board with the plastic containers is shielded from the mezzanine cards by an aluminum plate which is electrically connected to the outer Faraday cage. Right: sMDT signal distribution board with stacked mezzanine card mounted on the signal and ground pins of the drift tubes of a BMG chamber.

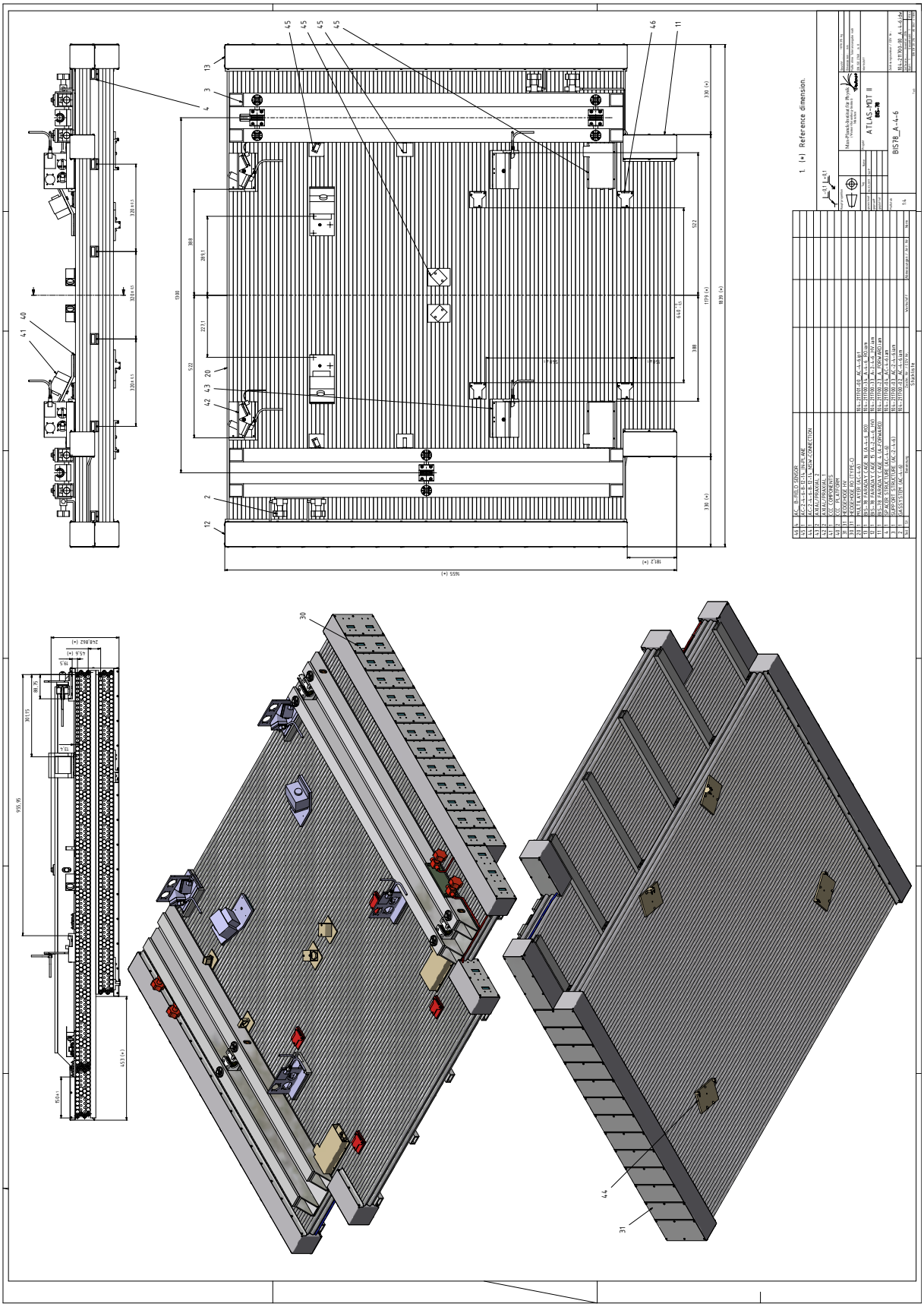

Figure 16: Drawings of a BIS 7/8 sMDT chamber with the alignment sensors mounted on platforms on the outside of the two multilayers.

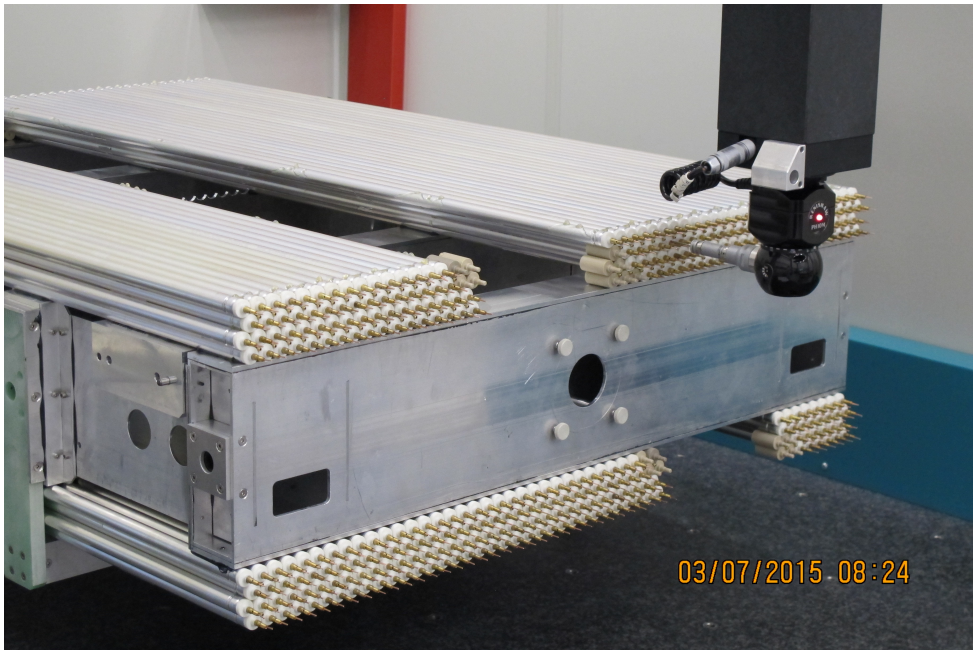

Figure 17: Measurement of the sense wire and alignment platform positions of a sMDT chamber with a Coordinate Measuring Machine (CMM). Individual wire positions are measured with an accuracy of 2 μm. The geometry parameters of the sense wire grids at the tube ends can be fully reconstructed. The wire positions on the readout and high-voltage distribution ends of the chamber are measured in the same coordinate frame allowing for the reconstruction of global deformations like torsion between the two ends.

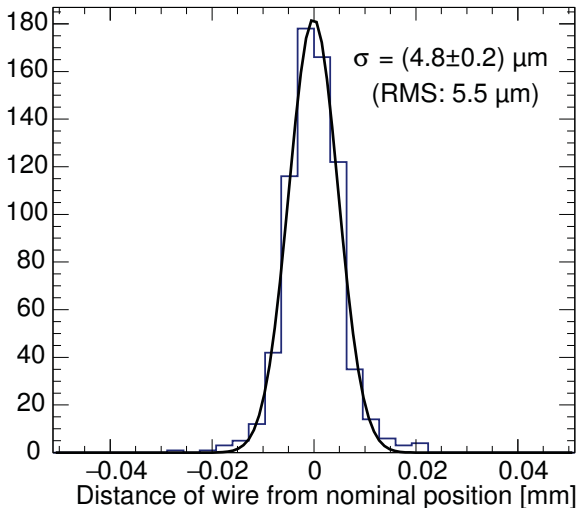

Figure 18: Residuals of the sense wire positions measured at both ends of a BMG sMDT chamber with 356 tubes with respect to the nominal wire grid. The width of the distribution includes the accuracy of the coordinate measureing machine of about 2 μm [5].

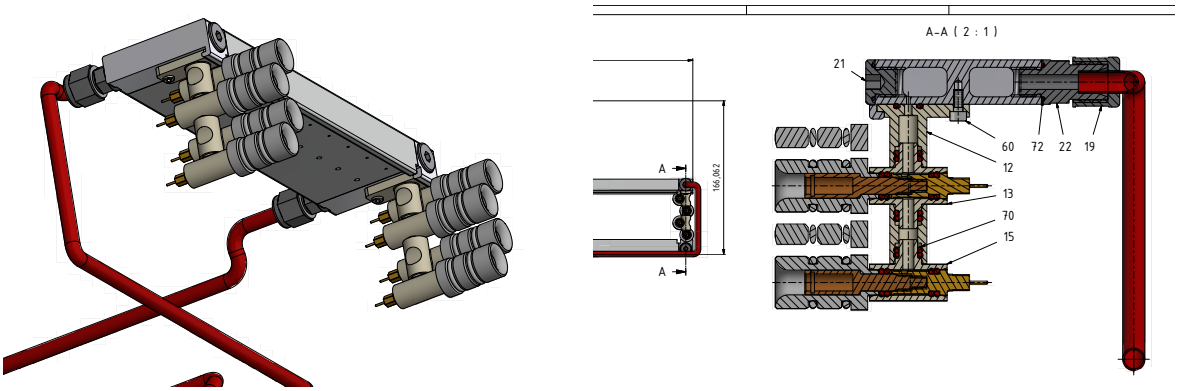

Figure 19: Schematics of the gas distribution system of the BIS 7/8 and BIS 1-6 sMDT chambers (left: 3D model, right: cross section). The principle is the same as for the BME and BMG chambers. It uses injection molded plastic gas connectors made of Crastin S600F20 (PBTB), the same materials as used for the endplug plastic parts [5] (see Figure 8), to connect the tubes in columns perpendiculat to the chamber plane to the aluminium gas bars mounted along each multilayer on the HV and RO side.

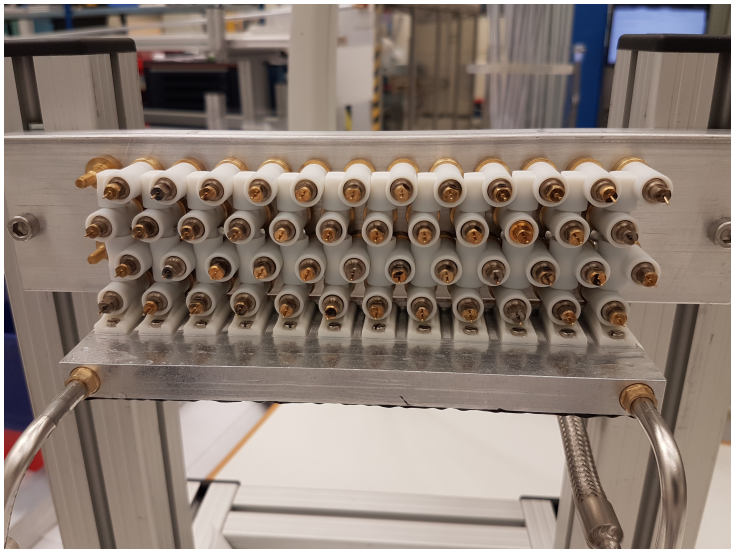

Figure 20: Test module of the BIS sMDT gas distribution system.

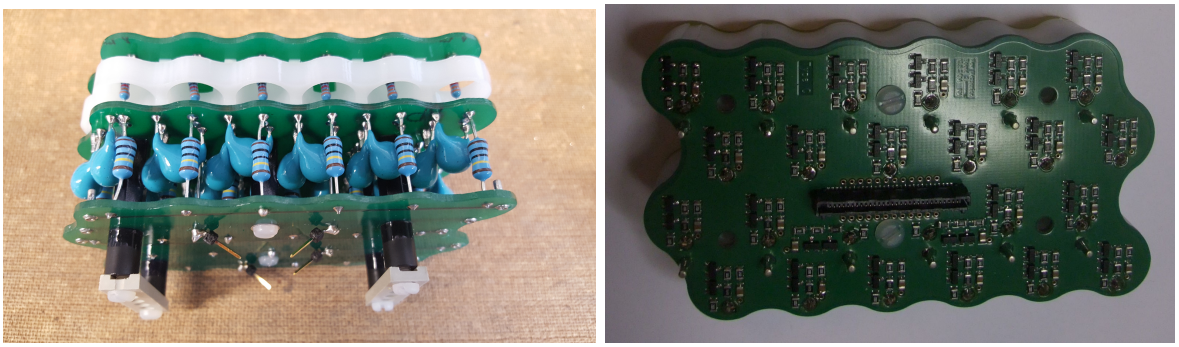

Figure 21: sMDT high-voltage (left) and signal (right) distribution (hedgehog) boards. The termination resistors on the high-voltage side and the coupling capacitors on the readout side are encapsulated in the injection molded white plastic containers in order to ensure HV stability.

Figure 22: HV distribution boards [2] for 6 x 4 channels mounted on the signal and ground pins of the drift tubes on the high-voltage side of a BMG chamber inside the Faraday cage.

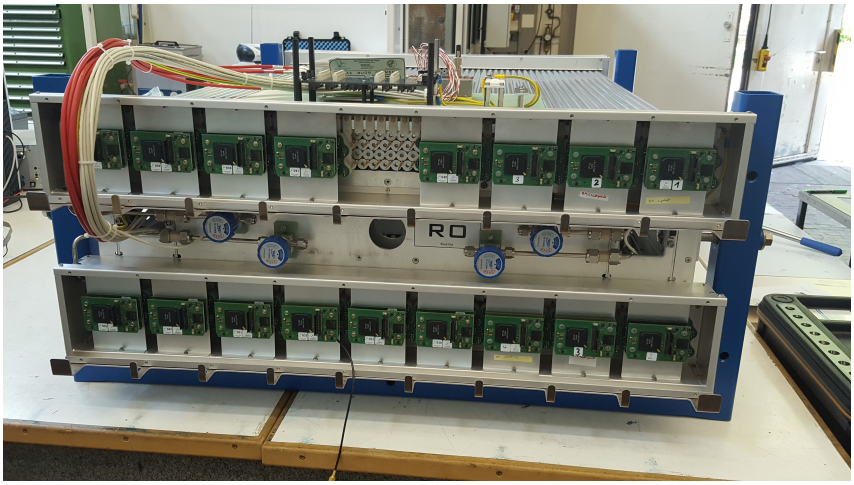

Figure 23: Signal distribution and active readout electronics (mezzanine) boards [11] with 6 x 4 channels mounted on the signal and ground pins of the drift tubes on the readout side of a BMG chamber inside the Faraday cage (see also Figure 15).

Figure 24: Readout side of sMDT chambers (BMG chambers during commissioning at CERN) with closed Faraday cages and flat (blue) twisted-pair signal cables connecting the mezzanine cards to the externally mounted readout boxes (CSMs).